https://doi.org/10.5194/amt-2021-42
Preprint. Discussion started: 4 March 2021

Atmospheric Measurement Techniques Discussions

Evaluation and Impact Factors of Doppler Wind Lidar during Super Typhoon Lekima (2019)

Xu WANG[1], Shengming TANG[2]*, Yun GUO[1], Jie TANG[2], Shuai Zhang[2]

[1]State Key Laboratory of Mountain Bridge and Tunnel Engineering, Chongqing Jiaotong University, 400074, China
[2]Shanghai Typhoon Institute of China Meteorological Administration, Shanghai 200030, China

Correspondence to: Shengming Tang (tangsm@typhoon.org.cn)

Abstract. Doppler wind lidar (DWL) has been shown to obtain fairly accurate wind speeds in normal wind conditions. However, the evaluation of DWL winds under typhoon conditions is less common. This study evaluated the accuracy of wind data measured by two types of DWLs (WindPrint S4000 and WindCube V2), and investigated the impact of factors (e.g., precipitation and humidity) on the DWL-observed wind speed and direction. Data were collected from joint observations in Baoshan, Zhoushan and Taizhou (China) by the Shanghai Typhoon Institute during the passage of Super Typhoon Lekima in 2019. The DWL observations were compared with measured data from balloon-borne radiosonde released at the same location. The results showed that the 1-min average wind speed and direction of WindPrint S4000 were more consistent with the instantaneous observation data of the sounding balloon than those of WindCube V2. The applicability of DWL was poor when the precipitation intensity was larger than 50 $mm \cdot h^{-1}$. The DWL wind speed bias significantly increased when the relative humidity exceeded 85%. When the drift distance of the sounding balloon (l_{drift}) was less than 1 km, the DWL wind speed bias decreased with an increase of l_{drift}, whereas it increased with an increase of l_{drift} when the drift exceeded 1.5 km. Within a radius of 700 km, the root mean square of wind speeds between DWL and sounding balloon measurements showed a trend of increasing as the distance from the typhoon center decreased.

Key words: Doppler wind lidar; typhoon; sounding; radiosonde; evaluation

1 Introduction

Typhoons are the most disastrous weather phenomenon in Southeast China. The boundary layer of a typhoon has been long recognized to be an important feature of the storm as it strongly constrains the distribution of energy, momentum and moisture in this region (Smith and Montgomery, 2010). However, typhoon winds, especially in the boundary layer, have been the least observed part of a typhoon until now (Zhang et al., 2018).

Traditional typhoon wind observation instruments such as anemometers, sounding balloons and Doppler wind profiler radar (WPR) have many limitations for measuring typhoon winds with high spatial and temporal resolution. Anemometers are

https://doi.org/10.5194/amt-2021-42
Preprint. Discussion started: 4 March 2021


Atmospheric Measurement Techniques Discussions

limited by the measurement height (usually <150 m) and poor maneuverability, while sounding balloons cannot hover accurately to obtain continuous observation data (Barat and cot, 1995). Doppler WPR is vulnerable to the interference of precipitation intensity (Ralph et al, 1995; Lambert and Taylor, 1998). By contrast, Doppler wind lidar (DWL) is characterized by high spatial-temporal resolution, strong anti-jamming capability and good mobility, which negates the traditional observation height limits (Hughes et al, 1972).

It was found that the DWL could obtain fairly accurate wind speeds compared with those from GPS sounding in the observation of -normal winds. For example, Kopp et al (1983) indicated that the observation results of continuous wave DWL were in good agreement with surface anemometers and with profiles measured by balloon sondes at heights of 100 m, 350 m and 750 m. The correlation coefficients of wind speed and wind direction were 0.83 and 0.91 respectively, and the root mean square (RMS) were only 1.3 $m \cdot s^{-1}$ and 12°. Roadcap et al (2001) pointed out that the CO_2 DWL had the same observation capability as sounding below a height of 6 km; the correlation coefficient of wind speed between them was more than 0.81, and the RMS was less than 1.95 $m \cdot s^{-1}$. Wolfe et al (2005) found that the correlation coefficient of wind speed between DWL and sounding below 1.5 km exceeded 0.97 and the speed accuracy of lidar reached 0.1 $m \cdot s^{-1}$. Kumer et al (2014) compared the winds observed by WindCube 100S and WindCube V1, and the results showed that the correlation coefficient of wind speed between WindCube 100S DWL and sounding was greater than 0.93 in the range 0.15–2.5 km. The correlation coefficient of wind speed between WindCube V1 DWL and sounding was greater than 0.7 in the range 70–250 m. Based on a data set of sounding observations, Li et al (2019) verified that the wind measurement error of Bistatic DWL radar was less than 1 $m \cdot s^{-1}$ within an altitude of 20 km. The above studies show that for normal winds observed by DWL, the correlation coefficient of wind speed is generally above 0.7 and the RMS is within 1–2 $m \cdot s^{-1}$, while the correlation coefficient of wind direction is high (>0.9) and the RMS is generally within 10°.

Under typhoon conditions, the evaluation of DWL is mainly carried by an aircraft over the sea. Pu et al (2010) analyzed the first observations of a typhoon by airborne DWL measurements, showing that the wind speed observed by airborne DWL and GPS dropsonde had good consistency within the range of 0–2 km from the surface, and the corresponding correlation coefficient and RMS values were 0.977 and 0.36 $m \cdot s^{-1}$, respectively. Bucci et al (2018) collected the wind observations from an airborne DWL from several tropical cyclones in 2016. Compared with the results from GPS dropsonde, they found that the

https://doi.org/10.5194/amt-2021-42
Preprint. Discussion started: 4 March 2021


Atmospheric Measurement Techniques Discussions

correlation coefficients of wind speed and wind direction reached 0.959 and 0.917 respectively, although the airborne DWL and GPS dropsonde locations were separated by 4.55 km on average. The average RMS values for wind speed and direction reached 10.27 $m \cdot s^{-1}$ and 40.66°, respectively. Zhang et al (2018) presented a verification of airborne DWL data collected during Tropical Storm Erika (2015). They found that the correlation coefficient and RMS between the DWL and dropsonde measurements were 0.95 and 1.58 $m \cdot s^{-1}$ within the range 0–1.4 km. Thus, for typhoon winds observed by a DWL over the sea, the above studies show that the correlation coefficients for wind speed and wind direction are generally above 0.95 and 0.90, respectively.

The wind measurement principle of a DWL relies on the inversion of the radial velocity by calculating the Doppler frequency shift of laser beams, which can be backscattered by atmospheric aerosol particles and atmospheric molecules (Korb et al, 1992). Therefore, the influence of external environmental factors on DWL performance, such as precipitation intensity, air humidity, and underlying surface topography, must be considered in measurement and research. Previous studies have indicated that precipitation could affect both the accuracy and range of DWL measurements. Roadcap et al (2001) pointed out that low humidity would reduce the backscattering of aerosol particles when they detected the wind speed using a CO_2 DWL and dropsondes. Träumner et al (2009) compared wind data collected by a scanning 2 μm Doppler lidar and a scanning 35.5 GHz cloud radar. They found that the average wind speed of DWL was larger than that obtained from the cloud radar during rain events. Davis et al (2013) analyzed DWL measurements in convective precipitation. They believed that precipitation caused the downward movement of aerosol particles, which led an increase of vertical velocity. However, the wind speed and precipitation intensity were relatively small in their observations, and no further quantitative analysis about the detection error of the DWL winds with the change of precipitation intensity was reported. Li et al (2020) used a shipborne micro-pulse lidar to measure the aerosol extinction coefficient over the South China Sea. They found that high humidity weakened the echo signal and they then carried out quality control of lidar measurements under high humidity conditions. However, there was no quantitative evaluation towards the impact of air humidity on the DWL winds.

It is worth mentioning that the wind data collected by balloon-borne radiosonde and DWL are not strictly observed at the same position. Sounding balloons drift with the wind during their ascent and collect instantaneous wind speeds at a fixed time interval. This leads to a deviation in wind measurements between the DWL and sounding balloons. However, in both normal

https://doi.org/10.5194/amt-2021-42
Preprint. Discussion started: 4 March 2021


Atmospheric Measurement Techniques Discussions

wind and typhoon conditions, the influence of the drift distance of a sounding balloon on the wind speed deviation of DWL was not considered in the above studies. Zhang et al (2018) used airborne DWL and dropsonde to observe the wind fields at different distances from the typhoon center and compared the vertical wind speed obtained from both instruments. The results showed that the agreement of vertical wind profiles between airborne DWL and dropsonde was generally good. However, the wind speed bias of DWL at different distances away from the typhoon center was not analyzed.

Based on joint observations during Super Typhoon Lekima in 2019 conducted by the Shanghai Typhoon Institute of China Meteorological Administration, this study reports on the first simultaneous typhoon observations with DWL and sounding balloons in China which were carried out at three observation locations—Baoshan, Zhoushan and Taizhou. The verification of the applicability and accuracy of wind data measured using a WindCube V2 DWL at Zhoushan were presented in Tang et al (2020). The current paper validates the wind measurements from different types of DWLs at three different observation locations. Moreover, by comparing the observed wind speed and direction data from the DWL and sounding balloons, this paper aimed to investigate the impact of precipitation, humidity, balloon drift distance and the position of the typhoon center on the wind speed (direction) deviation. The study will provide support for the use of DWL in tropical cyclone observations.

2. Joint observations during Super Typhoon Lekima

2.1 Super Typhoon Lekima (2019)

On August 4, 2019 (Beijing time is used throughout), typhoon Lekima formed east of the Philippines in the Northwest Pacific. On the evening of August 7, it intensified into a super typhoon. At 1:45 on August 10, it made landfall on the coast at Wenling City, Zhejiang Province, China. The maximum wind speed near the center was 52 m s^{-1} (super typhoon level), and the minimum sea-level pressure in the center was 930 hPa. After passing through Zhejiang Province and Jiangsu Province, Lekima moved into the western part of the Yellow Sea and made a second landfall on the coast of Huangdao District, Qingdao City, Shandong Province, China at 20:50 on August 11. It then crossed the Shandong peninsula into the Bohai Sea. The characteristics of Typhoon Lekima are as follows: (1) the intensity at landfall was the fifth largest in China's history, and the third largest in Zhejiang Province's history; (2) in total, rainfall records were broken at 19 stations in Zhejiang Province and

https://doi.org/10.5194/amt-2021-42
Preprint. Discussion started: 4 March 2021

Atmospheric Measurement Techniques Discussions

Jiangsu Province because of the heavy rainfall caused by the typhoon landfall and transit. During the typhoon, the average accumulated precipitation in Shandong and Zhejiang provinces reached 158 mm and 165 mm, the highest and second highest amounts in their history, respectively; (3) the typhoon's time over land ranked sixth in China's history, because of its long duration, wide range of influence and slow speed. The typhoon stayed for 20 hours in Zhejiang, which was its longest typhoon period. Figure 1 gives the path and intensity of Typhoon Lekima, and the positions of the three observation points. The path and intensity data for Typhoon Lekima are from the best track data of the Shanghai Typhoon Research Institute of China Meteorological Administration (Ying et al, 2014).

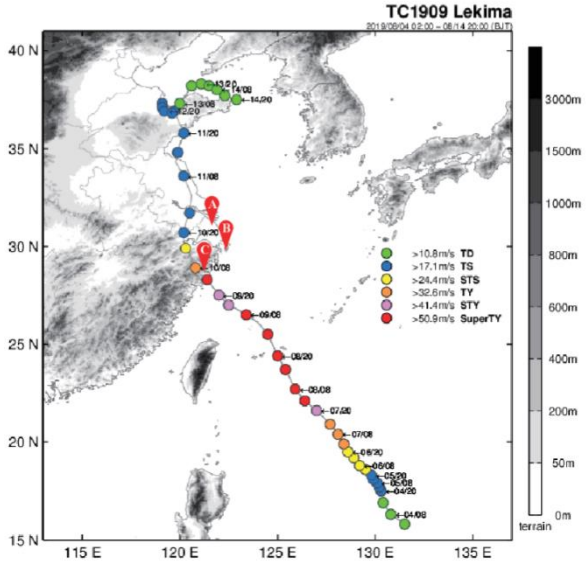

Figure 1: The track and intensity of Super Typhoon Lekima (2019) and locations of observation sites, where A represents Baoshan, B represents Zhoushan, and C represents Taizhou observation points. Different colors represent different typhoon intensities. TD: tropical depression; TS: tropical storm; STS: severe tropical storm; TY: typhoon; STY: severe typhoon; super TY: super typhoon. (Image courtesy to Xiping Zhang, Shanghai Typhoon Institute of China Meteorological Administration).

2.2 Joint observations

The joint observations were carried out at three sites at the same time, namely Baoshan, Taizhou and Zhoushan, as shown in Fig. 2. The Baoshan observation point was located in a suburb within the Baoshan District Meteorological Bureau of Shanghai, China (31.3908° N, 121.4446° E). To the south of the observation site the land was flat with few buildings, while to

https://doi.org/10.5194/amt-2021-42
Preprint. Discussion started: 4 March 2021

Atmospheric Measurement Techniques Discussions

the north, west and east it was densely populated with many buildings. The shortest distance between the typhoon center and the test site was about 99 km during the typhoon. The Zhoushan observation point was located at Zhoushan International Cruise Port (29.9022°N, 122.3674°E), with farmland and a few buildings to the north and east, belonging to a flat suburban landform, adjacent to the Zhitou Ocean in the south. The shortest distance between the typhoon center and the test site was about 164 km. The Taizhou observation site was located in a vacant lot on the east side of a football field at Hongjia Central Primary School in Jiaojiang District, Taizhou City, Zhejiang Province (28.6180° N, 121.4166° E). There were a few buildings to the east of the field, and dense urban buildings to the north, west and south. The shortest distance between the typhoon center and the test site was about 36 km.

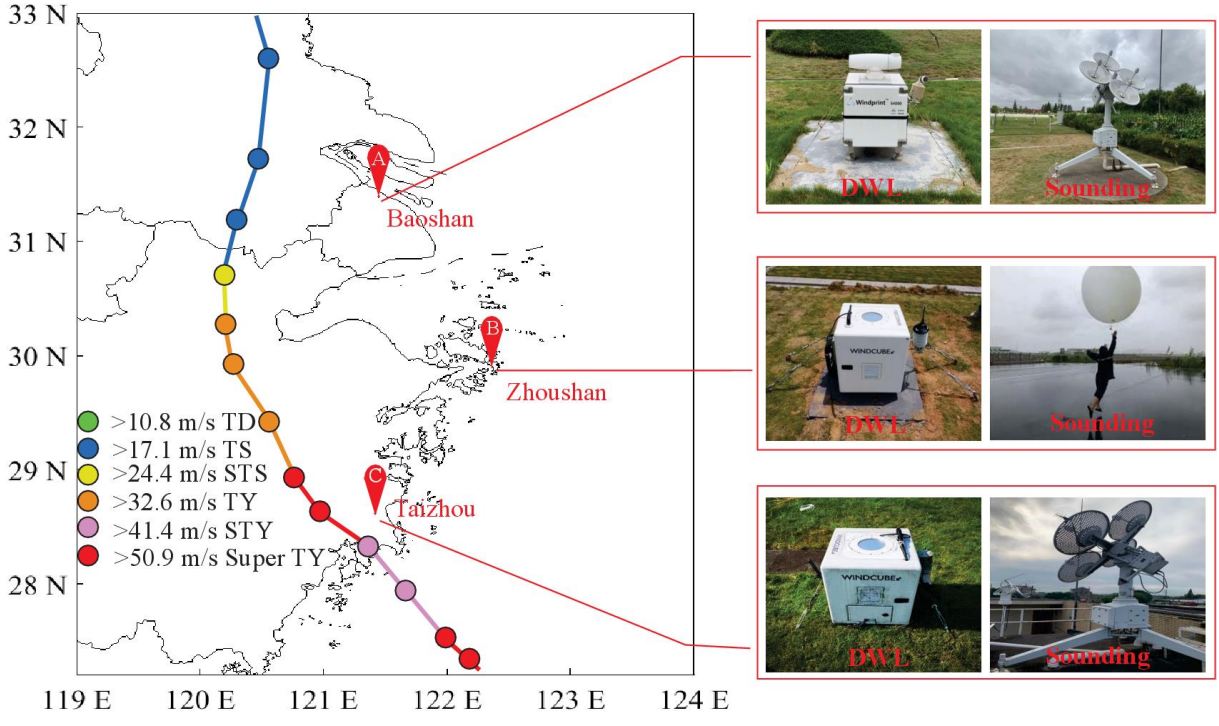

Figure 2: Locations and local surroundings of the three observation sites in the joint observations, and the field operation photographs for DWLs and soundings. A represents Baoshan, B represents Zhoushan, and C represents Taizhou observation points.

https://doi.org/10.5194/amt-2021-42
Preprint. Discussion started: 4 March 2021


Atmospheric Measurement Techniques Discussions

3 Instruments

3.1 Instrument setup

3.1.1 DWL

The DWL at Baoshan observation point used WindPrint S4000 3D scanning coherent Doppler lidar produced by Qingdao Huahang Environmental Technology Co., Ltd in China. According to the equipment description, the lidar works in the infrared band, and can detect the atmospheric wind field from the ground to an altitude of 4000 m, with a high temporal resolution (about 0.25 Hz). The accuracy of the horizontal wind speed under normal environmental conditions is less than 0.1 m s^{-1}. A variety of atmospheric parameters, such as radial wind speed, horizontal wind speed, wind direction, vertical wind speed, signal-to-noise ratio (SNR), ground temperature and air pressure, can be obtained continuously. A total of 152 layers were set in the vertical height measurement.

The DWL in Zhoushan and Taizhou adopted WindCube V2, a professional wind-measuring lidar developed by the French company, Leosphere. It can continuously measure the wind speed and direction, SNR, temperature, humidity and air pressure of surrounding ground in the height range 0–300 m. The vertical height of the survey was set up with 12 layers, which were 40 m, 50 m, 70 m, 100 m, 130 m, 150 m, 180 m, 200 m, 230 m, 250 m, 270 m and 290 m, respectively.

3.1.2 Radiosonde

In the typhoon joint observations, sounding balloons were released at the same place as the DWL observations to compare their measurements. The GTS1 digital radiosonde was used in Baoshan and Taizhou observation points. This sonde is a new digital high-altitude detection instrument developed by the Shanghai Changwang Meteorological Science and Technology Company. It can continuously track, locate and measure the trajectory of the sounding balloon through GFE (L) 1 (L-band radar) secondary wind-finding radar (Fig. 2). The wind data were obtained by mathematical model calculations within the specified time interval (1 s) The radar receiver receives the radiosonde code from the radiosonde continuously, and compiles the radiosonde data, namely atmospheric temperature, air pressure, humidity and other meteorological elements. A Vaisala RS41-SG radiosonde was used in Zhoushan station, which was developed by Vaisala Company in Finland. It uses a GPS positioning system to calculate the atmospheric wind speed, wind direction, detection height and real-time longitude and

https://doi.org/10.5194/amt-2021-42
Preprint. Discussion started: 4 March 2021


Atmospheric Measurement Techniques Discussions

latitude information according to the position change of the instrument and uses a digital measurement circuit to measure atmospheric temperature, air pressure and humidity.

The types of measuring instruments and the observation start and end time in three sites are summarized in Table 1. The detailed measurement parameters of the DWLs and radiosondes are listed in Table 2.

Table 1: Instrument models and observation time in three locations

location	DWL	Radiosonde	Observation start and end time
Baoshan	WindPrint S4000	GTS1	2019.08.09_00:00~2019.08.10_17:00
Zhoushan	WindCube V2	Vaisala RS41-SG	2019.08.09_13:00~2019.08.10_13:00
Taizhou	WindCube V2	GTS1	2019.08.08_00:00~2019.08.10_24:00

Table 2: Measurement parameters of DWLs and radiosondes

Parameter	DWL (WindCube V2)	DWL (WindPrint S4000)	Radiosonde (Vaisala RS41-SG)	Radiosonde (GFE(L)1-GTS1)
Range	40~290 m	0~4 km	0~40 km	0~3000 km
Data sampling rate	1 Hz	0.25Hz	0.5 Hz	1 Hz
Speed accuracy	0.1 $m·s^{-1}$	0.1 $m·s^{-1}$	0.1 $m·s^{-1}$	1 $m·s^{-1}$ (<10 $m·s^{-1}$) 10% (>10 $m·s^{-1}$)
Speed range	0~80 $m·s^{-1}$	0~75 $m·s^{-1}$	0~160 $m·s^{-1}$	0~200 $m·s^{-1}$
Direction accuracy	1°	0.1°	0.1°	5° (<25 $m·s^{-1}$) 10° (>25 $m·s^{-1}$)
Beam geometry	4 inclined beams at 28° + 1 vertical beam	4 inclined beams at 60° + 1 vertical beam	—	—
Wavelength	1543 nm	1550 nm	—	—

https://doi.org/10.5194/amt-2021-42
Preprint. Discussion started: 4 March 2021

Atmospheric Measurement Techniques Discussions

Temperature range	− 35 ~ +45 °C	− 50 ~ +85 °C	–90 ~ +60 °C	–90 ~ +50 °C
Humidity range	0%~100% RH	0%~100% RH	0%~100% RH	0%~100% RH

3.2 Measurement principle of DWL

A Doppler beam swinging (DBS) 5 beam scanning method was used for wind field observations for both WindCube V2 and WindPrint S4000, as shown in Fig. 3. Compared with the velocity-azimuth display method which uses a complete cone scan to collect dense radial wind speed data (Holleman, 2005), the DBS scanning mode has a shorter scanning time.

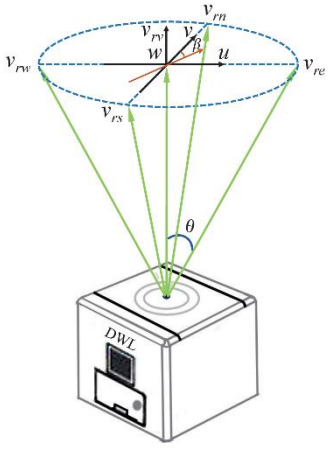

Figure 3: Schematic diagram of the wind measurement principle for DWL, where v_{re}, v_{rs}, v_{rw}, and v_{rn} represent radial wind speed in the east, south, west and north, respectively. v_{re} is the wind speed on the vertical beam; u, v, w are the velocity components of the circle center in Cartesian coordinates (x, y, z); and β is the horizontal wind direction. θ is the zenith angle of laser beam scanning.

The measurement principle of DWL adopts the principles of laser pulse Doppler frequency shift. The lidar emits a laser pulse to the atmosphere and receives a backscattering echo signal from atmosphere. The relationship between the Doppler frequency shift and the lidar radial wind speed is as follows:

$$v_r = \lambda \Delta f / 2, \quad (1)$$

where v_r is the radial wind speed; λ is the laser wavelength, where λ of WindCube V2 is 1543 nm and that of WindPrint S4000 is 1550 nm; Δf is the Doppler frequency shift.

In fact, the radial wind was directly measured by DWL. The laser beams were emitted from five directions. Four laser beams were scanned upward in the zenith angle from the direction of east, south, west and north. The middle laser beam

https://doi.org/10.5194/amt-2021-42
Preprint. Discussion started: 4 March 2021


Atmospheric Measurement Techniques Discussions

pointed vertically to the zenith (Fig. 3). The Doppler frequency shift produced by the laser beam in the scattering of atmospheric aerosol particles was measured, and then the radial wind speed in the direction of laser emission was retrieved. The horizontal wind field and the required data products were obtained by the following methods.

Under the assumption that the horizontal wind field has a linear distribution, the wind speed information of each radial direction was obtained using DWL. The three-dimensional wind speed component at the center of the circle was obtained by taking the radial wind speed in each direction and using the trigonometric function relationship:

$$\begin{bmatrix} u \\ v \\ w \end{bmatrix}^T = \begin{bmatrix} v_{re} \\ v_{rw} \\ v_{rn} \\ v_{rs} \\ v_{rv} \end{bmatrix}^T \begin{bmatrix} \frac{1}{\sin\theta} & 0 & 0 \\ -\frac{1}{\sin\theta} & 0 & 0 \\ 0 & \frac{1}{\sin\theta} & 0 \\ 0 & -\frac{1}{\sin\theta} & 0 \\ 0 & 0 & 1 \end{bmatrix}, \quad (2)$$

where u, v and w are wind components in the Cartesian coordinates (x, y, z), θ is the zenith angle, which represents the angle between the lidar beam and the vertical direction. The wind speed and direction in the horizontal direction can then be obtained as:

$$U = \sqrt{u^2 + v^2}, \quad (3)$$

$$\beta = arctan(u/v), \quad (4)$$

where U is the horizontal total wind speed, and β is the horizontal wind direction, rotating clockwise from due north (0°).

4 Evaluation

To evaluate the DWL observation data under typhoon conditions using a sounding balloon, first quality control of the DWL observation data was carried out. According to Goit et al (2020), quality control with 80% data efficiency can significantly reduce the RMS of wind speed observed by DWL. Therefore, referring to the research of Goit et al (2020), this paper took the effective rate of 1 min data as the threshold value, and a data efficiency below 80% was recorded as data missing. Quality control of the DWL measured data of Baoshan, Zhoushan and Taizhou was carried out, and the 1 min mean horizontal wind speed (U), wind direction, the data missing rate and precipitation intensity (I) with time were plotted, as shown in Fig. 4.

https://doi.org/10.5194/amt-2021-42
Preprint. Discussion started: 4 March 2021

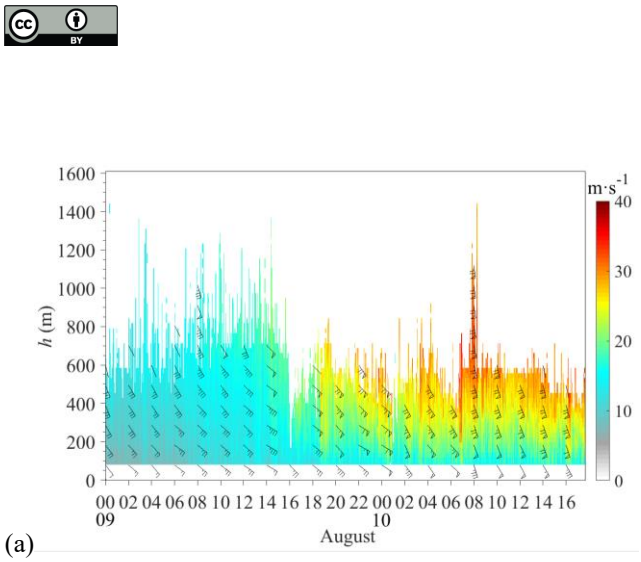

(a)

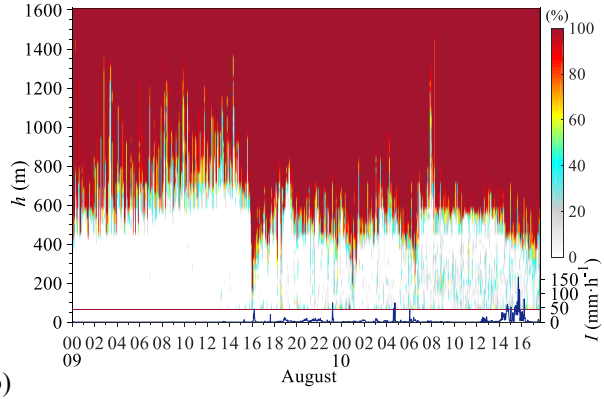

(b)

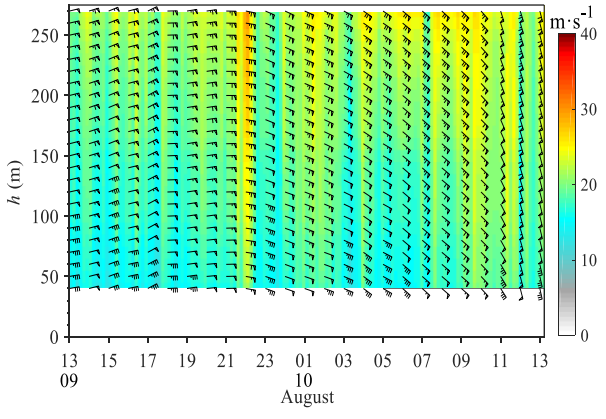

(c)

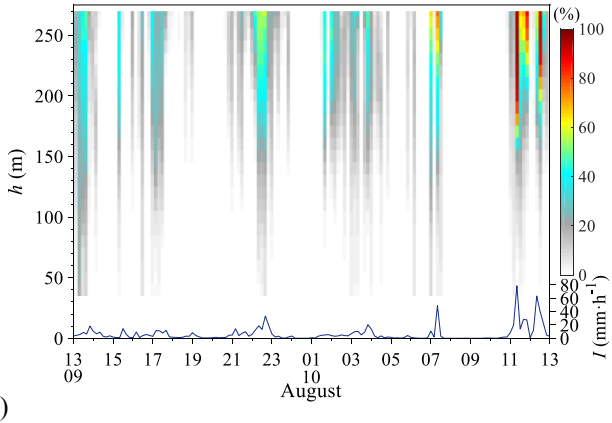

(d)

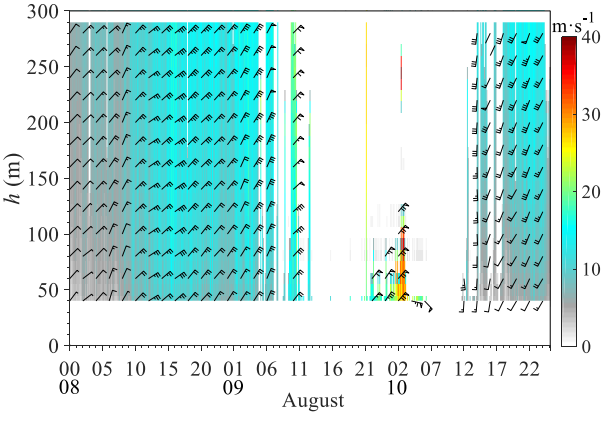

(e)

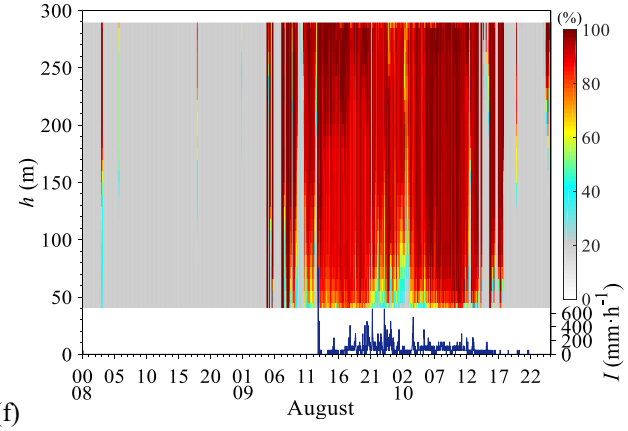

(f)

Figure 4: Variation of (a, c, e) 1-min average horizontal wind speed and wind direction, and (b, d, f) 1-min data missing rate of DWL measurements with time at different altitudes. (a–b) represent Baoshan observation point, (c–d) represent Zhoushan observation point, and (e–f) represent Taizhou observation point.

https://doi.org/10.5194/amt-2021-42
Preprint. Discussion started: 4 March 2021


Atmospheric Measurement Techniques Discussions

From the changes of wind speed in Fig. 4 (a), (c) and (e), it can be seen that the DWL measured *U* in Baoshan was basically less than 20 m s^{-1} before 16:00 on August 9. After that, the average wind speed began to increase significantly and reached its maximum value (35 m·s^{-1}) at 07:00 on August 10. In terms of wind direction, before 00:00 on August 10, the wind at the measured site was a southeast wind. Then the wind direction clearly changed from southeast to south, which was mainly because the typhoon center of Lekima moved north after landfall. The *U* of Zhoushan station reached its maximum (30.6 m·s^{-1}) about 4 hours before the typhoon made landfall (21:50 on August 9). In terms of wind direction, before 21:50 on August 9, the wind at Zhoushan was an east wind, and this gradually changed to a south wind. During the period from 11:00 on August 9 to 14:00 on August 10 in Taizhou, the data for wind speed and direction were missing, and the maximum wind speed was about 35 m s^{-1}. The wind direction was north before 02:00 on August 10, and then changed sharply to south.

Inspection of data efficiency (Fig. 4 (b), (d), (f)) shows that the rate of missing DWL data increased with the increase of height. Generally, the greater *I* was, the greater the data missing rate became. The missing rate of the DWL measured data below 200 m in Baoshan was less than 20%, and that of data above 800 m was 100%. After 16:00 on August 9, because of the obvious increase of *I*, the rate of missing DWL data increased significantly. When *I* was greater than 50 mm h^{-1} (16:20 on August 9 and 01:00 on August 10), the missing rate of data above 200 m was as high as 100% (Fig. 4b). The data missing rate of the Zhoushan observation point was less than 20% when the height was below 100 m. However, the data missing rate was high when the height was more than 200 m. In some time periods, such as 11:30 on August 10 (I>50 mm·h^{-1}), the missing rate of data above 200 m was as high as 100% (Fig. 4d). When *I* was small or there was no precipitation (before 12:00 on August 9), the data missing rate of the Taizhou observation point was less than 20%. However, when the precipitation intensity was high (I>50 mm·h^{-1}), the missing rate of DWL data was more than 80% (Fig. 4f). The above analyses show that the applicability of DWL is poor when the precipitation intensity is greater than 50 mm·h^{-1}.

From the observation results of DWL at the three observation points, it can be seen that the observation capacity of both WindPrint S4000 and WindCube V2 DWL was reduced under precipitation conditions, and the data missing rate increased significantly. It can be seen from Fig. 4 (b), (d) and (f) that when there was no precipitation or when the precipitation intensity was small, the data missing rate was basically less than 20%. When the precipitation intensity I>50 mm s^{-1}, the data missing rate above 200 m height began to increase rapidly with height, and the data missing rate was as high as 100%. One possible

https://doi.org/10.5194/amt-2021-42
Preprint. Discussion started: 4 March 2021


Atmospheric Measurement Techniques Discussions

reason for the missing data was that with the increase of detection height, aerosol particles decreased, resulting in a decrease of the angular scattering probability of lidar—the continuous weakening of the echo signal resulted in data missing. Another reason may be related to precipitation, whereby heavy rainfall accumulating on the window surface led to a decrease of the atmospheric transmission of laser light, which continuously weakened the echo signal. In general, except for the Taizhou observation point, the data missing rate of WindPrint S4000 and WindCube V2 DWL was mostly less than 20%, which means the observation data had a data efficiency greater than 80%.

Because there is a lack of research evaluating the DWL-derived wind velocity deviation under typhoon and heavy rainfall conditions, it was necessary to evaluate the accuracy and validity of the typhoon wind field data measured by DWL in this joint observation experiment. Owing to the high reliability of radiosonde in the measurement of the wind field under typhoon and heavy rainfall conditions, many previous studies have used sounding data to evaluate the performance of DWL wind measurements (Barat and Cot, 1995; Pu et al, 2010; Zhang et al, 2018; Tang et al, 2020). In this study, sounding balloons were released at the same observation sites, and the measured data of the sounding balloon was used to evaluate the observation deviation of DWL. Altogether, data from 17 sounding balloons at three observation points were analyzed. Five sounding balloons were initially released at the Baoshan observation point at 01:15, 07:15 and 19:15 on August 9, and 01:17 and 07:42 on August 10. The initial release time of nine sounding balloons at the Zhoushan observation point was 14:59, 17:12, 19:18, 21:23 and 23:58 on August 9 and 02:22, 05:34, 07:07 and 11:50 on August 10. Three sounding balloons were released at the Taizhou observation point at 07:15 and 19:15 on August 8 and 19:15 on August 10, respectively.

It should be noted that the wind speed observed by DWL and sounding balloon was not an identical in situ observation in the strict sense. On the one hand, the sounding balloons drifted with the wind in the process of rising and gradually moved away from the release point. The observed wind speed was the instantaneous wind speed at different heights collected at a fixed time frequency (1 s). On the other hand, the larger the tilt beam zenith angle of lidar (θ) was, the higher the measurement accuracy became, and the horizontal range of measurement also increased. Under highly turbulent wind conditions, the assumption that the atmospheric horizontal wind field is linearly distributed is difficult to meet. In addition, owing to the high measurement accuracy and small time-delay inertial coefficient of lidar, the observation data contained high-frequency pulsation caused by atmospheric turbulence, which caused large wind speed measurement deviations in the typhoon boundary

https://doi.org/10.5194/amt-2021-42
Preprint. Discussion started: 4 March 2021


Atmospheric Measurement Techniques Discussions

layer where the atmospheric turbulence is active (Gasch et al, 2020). Therefore, in practice, the average wind speed in a certain time period is used to avoid the wind measurement deviations caused by the changes of atmospheric turbulence. For example, Drew et al (2013) used the average wind speed of 1 h to study the average wind speed profile during the whole observation period (4578 h) of lidar. Li and Yu (2017) and Li et al (2018) used 10-min average wind speed to evaluate the potential of coastal wind resources in Lake Erie. In this study, the average wind speeds of DWL measured in 30 s, 1 min and t_{GPS} (the time of the balloon drifting to the maximum observation height of lidar) were selected to evaluate the consistency degree with the measured instantaneous wind speed of sounding balloon.

Figure 5 shows the comparison of horizontal wind velocity measured at different heights between the WindPrint S4000 DWL and GTS1 radiosonde at the Baoshan observation point, and the drift distance of the sounding balloon over time (l_{drift}). As can be seen from the figure, below 100 m, the DWL-measured wind speed was significantly greater than that of the sounding balloon. With the increasing height of the sounding balloon, the gap between them became smaller and smaller. When the height reached above 100 m, there was a crossover for wind speed between the DWL and sounding balloon measurements, and the observed results were basically the same. This was because the release of sounding balloon made it accelerate from a static position. The wind speed value observed by sounding balloon from static to complete drift with the wind was basically less than the real wind speed value, causing a deviation in wind speed measurement. As with the results of Zhang et al (2018) and Tang et al (2020), the drift effect of the balloon-borne radiosonde was the main reason for the large wind speed deviation below 100 m. When the height reached about 100 m, the sounding balloon ended the initial acceleration and began to drift completely with the wind, so it was in good agreement with the DWL measurements. Therefore, this paper considered that the measured data of sounding balloons below 100 m were not credible. In addition, the horizontal distance between the sounding balloon at the maximum observation height of DWL (600 m) and the release point was within 12 km. In general, the trends of average wind speed in 30 s, 1 min and t_{GPS} in vertical height were the same.

https://doi.org/10.5194/amt-2021-42
Preprint. Discussion started: 4 March 2021

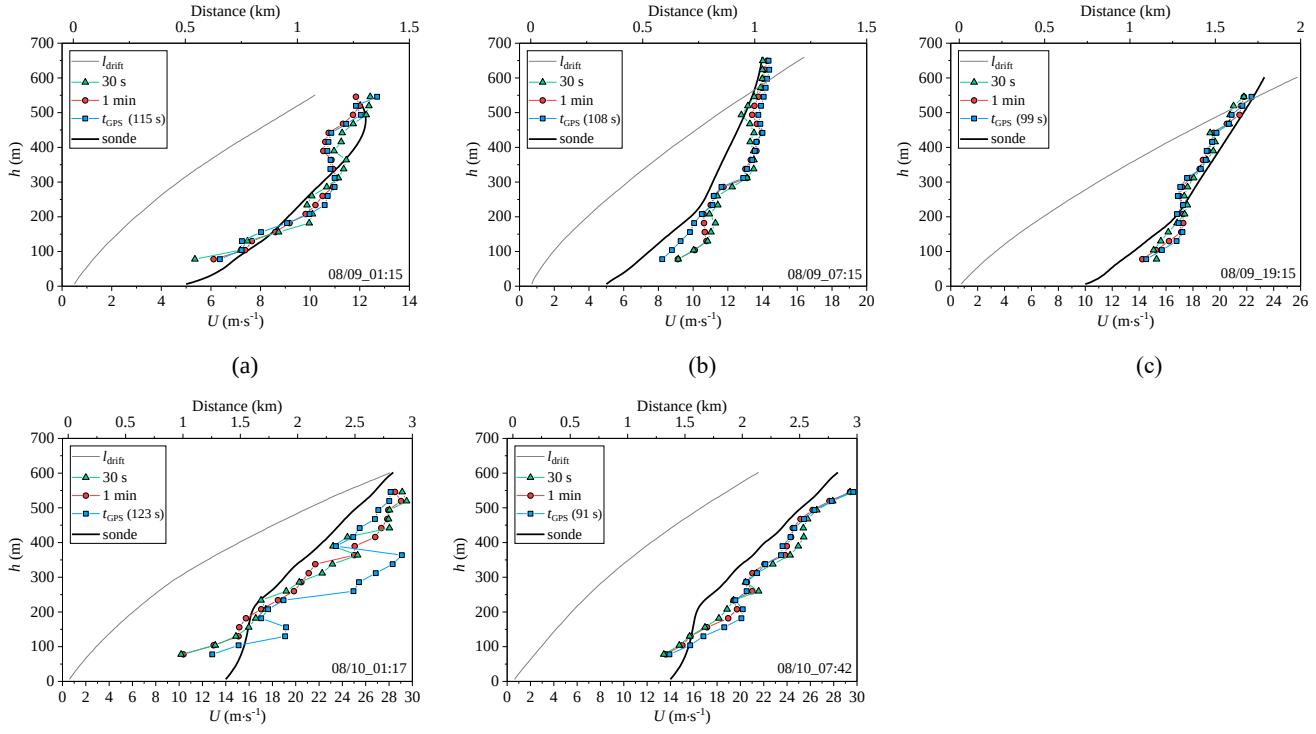

Figure 5: Comparison of horizontal wind speeds between WindPrint S4000 DWL and GTS1 radiosonde at the Baoshan observation point. l_{drift} represents the drift distance of the balloon-borne radiosonde during ascent; 30 s, 1 min and t_{GPS} represent 30-s, 1-min and t_{GPS} average DWL-derived wind speeds, respectively; and sonde represents the measured wind speed of the GTS1 radiosonde. (a)–(e) correspond to 01:15, 07:15 and 19:15 on August 9 and 01:17 and 07:42 on August 10, respectively.

Figure 6 shows the comparison of the measured horizontal wind speeds at different heights between the WindCube V2 DWL and the GPS sounding balloon, and the horizontal distances of the sounding balloon from the initial release point at different heights at the Zhoushan observation point. Like the Baoshan observation point, the sounding balloon has a drift effect below 100 m height. Through careful observation of Fig. 6(f) and Fig. 6(g), it can be seen that the velocity of the sounding balloon suddenly increased at a height of 100 m at 02:02 and 180 m at 05:34 on August 10, and the height of sounding balloon remained unchanged for a period of time (about 10–15 s), although the horizontal drift distance l_{drift} increased. This was due to the influence of a low-altitude jet or turbulence, resulting in a sudden increase of the horizontal instantaneous velocity of the sounding balloon. However, because the wind speeds in 30 s, 1 min and t_{GPS} were averages, the change of low-altitude jet or turbulence cannot be well captured. At the same time, owing to the inertial acceleration, the observed wind speed of the

https://doi.org/10.5194/amt-2021-42
Preprint. Discussion started: 4 March 2021

Atmospheric Measurement Techniques Discussions

sounding balloon was generally faster than that of DWL. In addition, the horizontal distance between the sounding balloon and its release point at the maximum observation height (270 m) of DWL was within 0.9–1.6 km. On the whole, the variation trends of average wind speed of DWL over 30 s, 1 min and t_{GPS} in the vertical height were similar, but the t_{GPS} average wind speed was closest to that of sounding balloon.

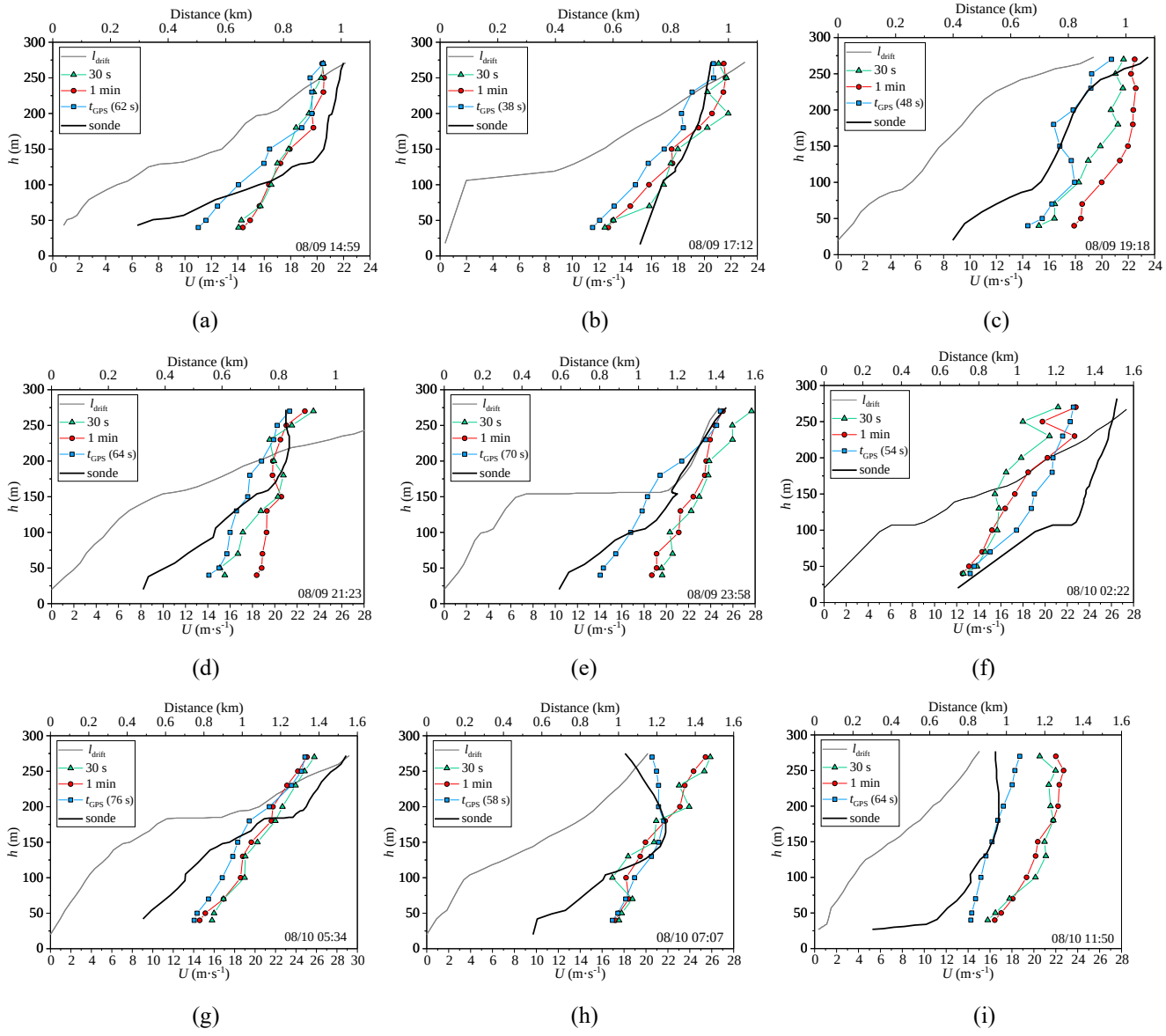

Figure 6: Comparison of horizontal wind speeds between WindCube V2 DWL and GPS sounding at the Zhoushan observation point. l_{drift} represents the drift distance of the balloon-borne radiosonde during ascent, 30 s, 1 min and t_{GPS} represent 30-s, 1-min and t_{GPS} average DWL-derived wind speeds, respectively, and sonde represents the measured wind speed of the GPS sounding. (a)–(i)

https://doi.org/10.5194/amt-2021-42
Preprint. Discussion started: 4 March 2021

Atmospheric Measurement Techniques Discussions

correspond to 14:59, 17:12, 19:18, 21:23 and 23:58 on 9 August and 02:22, 05:34, 07:07 and 11:50 on 10 August, respectively.

Owing to the large data missing of WindCube V2 DWL at the Taizhou observation point from 11:00 on August 9 to 14:00 on August 10 (Fig. 4f), it was impossible to compare it with the wind speed observed by sounding balloon. Therefore, Fig. 7 only shows the comparison of the measured horizontal wind speed at different heights between the DWL and the sounding balloon at three time points at the Taizhou observation point. It can be seen from the figure that the wind speeds of the three time points were small (U<15 m·s^{-1}). Similar to the Baoshan and Zhoushan observation points, the sounding balloon had a drift effect below 100 m. The horizontal distance between the point where sounding balloon was at the maximum observation height (290 m) and the release point was less than 600 m.

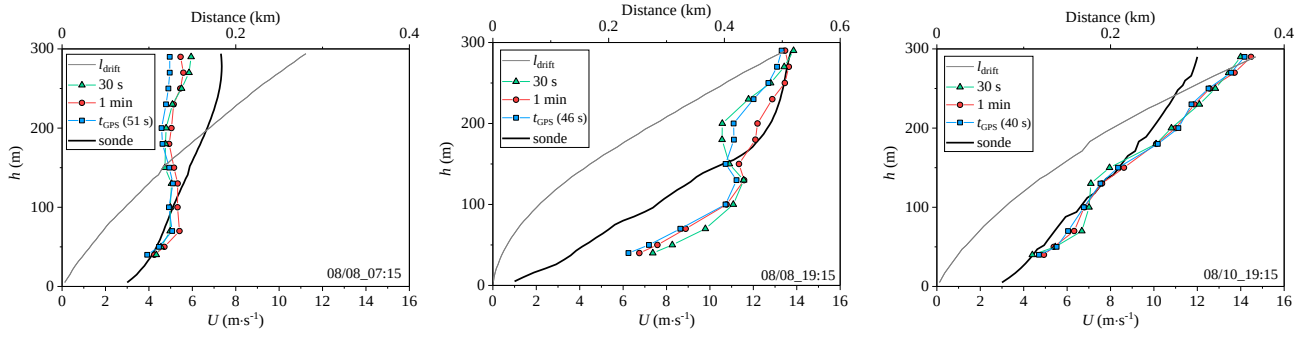

Figure 7: Comparison of horizontal wind speeds between WindCube V2 DWL and GTS1 radiosonde at the Taizhou observation point. l_{drift} represents the drift distance of the balloon-borne radiosonde during ascent, 30 s, 1 min and t_{GPS} represent 30-s, 1-min and t_{GPS} average DWL-derived wind speeds, respectively, and sonde represents the measured wind speed of the GTS1 radiosonde. (a)–(c) correspond to 07:15 and 19:15 on August 8 and 02:22 and 19:15 on August 10, respectively.

To quantitatively describe the consistency of measured wind speed between DWL and the sounding balloons, statistical parameters including RMS and R (correlation coefficient) were calculated based on the 30-s, 1-min and t_{GPS} average wind speed and direction of DWL and the instantaneous wind speed and direction of the sounding balloons at the Baoshan, Zhoushan and Taizhou observation points. The results are listed in Table 3. At the Baoshan observation point, it can be seen from both RMS (1.29 m·s^{-1}) and R (0.98) that the average wind speed in 1 min from WindPrint S4000 DWL was better than that in 30 s and in t_{GPS}, and it was also better than the comparison results of DWL and sounding balloon under the condition of normal winds measured by Kopp et al (1983) and Roadcap et al (2001) (RMS were 1.3 m·s^{-1} and 1.95 m·s^{-1}, R were 0.83 and 0.81,

https://doi.org/10.5194/amt-2021-42
Preprint. Discussion started: 4 March 2021


Atmospheric Measurement Techniques Discussions

respectively). The values were also better than the observed comparison results of Tropical Storm Erika (2015) by Zhang et al. (2018) (RMS was 1.58 m·s^{-1}, R was 0.95). The average wind speed in t_{GPS} (R were 0.90 and 0.82, RMS were 1.52 m·s^{-1} and 2.19 m·s^{-1}, respectively) of WindCube V2 DWL at the Taizhou and Zhoushan observation points was closer to the wind speed measured by sounding balloon than that in 30 s and 1 min, but it was bigger than the observation results of Typhoon Nuri (2008) by Pu et al. (2010) (RMS was 1.087 m·s^{-1}, R was 0.977). This may be because Pu et al. (2010) used airborne Doppler radar and dropsonde which made the observation accuracy higher. Looking at the wind direction, it can be seen from Table 3 that the average wind directions in t_{GPS} of the three observation points were in good agreement with the wind directions measured by sounding balloon: the minimum value of RMS was 2.56°, 6.99° and 12.97°, and all the values of R exceeded 0.95. Owing to the different length of each t_{GPS}, it was impossible to compare these in a unified standard. Through comparison, the differences between the RMS and R of mean wind speed and direction in 1 min and t_{GPS} were small. Considered comprehensively, the 1-min average wind speed and direction were adopted for further research in this paper.

By comparing the RMS and R of wind speed measured by WindPrint S4000, WindCube V2 and sounding balloon, the coincidence degree of wind speed with sounding balloon measured by WindPrint S4000 in Baoshan was higher than that measured by WindCube V2 in Zhoushan and Taizhou. This may be because the Baoshan observation point was far from the typhoon landfall center and, therefore, the wind speed and precipitation intensity were small.

Table 3 Correlation coefficient (R) and root mean square (RMS) of 30-s, 1-min and t_{GPS} average wind speeds and wind directions between DWL and sounding measurements at Baoshan, Zhoushan and Taizhou observation points.

		RMS (m·s^{-1}) (30 s)	R (30 s)	RMS (m·s^{-1}) (1 min)	R (1 min)	RMS (m·s^{-1}) (t_{GPS})	R (t_{GPS})
Baoshan	Speed	1.34	0.98	1.29	0.98	1.79	0.96
	Direction	3.47	0.92	2.85	0.94	2.56	0.96
Zhoushan	Speed	3.98	0.65	3.47	0.71	2.19	0.82
	Direction	15.32	0.91	14.07	0.92	12.97	0.96
Taizhou	Speed	2.33	0.95	1.79	0.97	1.52	0.90
	Direction	9.42	0.99	7.43	0.99	6.99	0.99

https://doi.org/10.5194/amt-2021-42
Preprint. Discussion started: 4 March 2021


Atmospheric Measurement Techniques Discussions

5 Impact factors

5.1 Precipitation

To reveal the influence of typhoon precipitation on wind field observations of DWL, the SNR and data missing rate under precipitation conditions were studied. First, the WindPrint S4000 DWL at Baoshan observation point was divided into four layers according to the observation height: ≤200 m, 200–400 m, 400–600 m and 600–800 m. The WindCube V2 DWL at the Zhoushan and Taizhou observation points were divided into three layers according to the observation height: ≤100 m, 100–200 m and 200–290 m. According to the group standard T/CMSA0013-2019 (2019), the precipitation intensity was divided into seven grades: 0–0.01 mm·h^{-1} (sunny), 0.01–3 mm·h^{-1} (light rain), 3–6 mm·h^{-1} (moderate rain), 6–12 mm·h^{-1} (heavy rain), 12–30 mm·h^{-1} (rainstorm), 30–90 mm·h^{-1} (heavy rainstorm), and above 90 mm·h^{-1} (severe rainstorm). The variation of 1-min average SNR with *I* of the two lidars is shown in Fig. 8. The figure shows that *I* has different effects on the SNR at different heights, and that the SNR decreases with an increase of *I*, which is consistent with the findings reported by Tang et al (2020). Inspection of Fig. 8(a) suggests that the SNR of the WindPrint S4000 DWL at the Baoshan observation point did not change with *I* below 600 m and was between 2–4 dB. The SNR decreased with the increase of *I* when the height was over 600 m, and the effect was more obvious. Under the conditions of *I* of 0.013 mm·h^{-1} (light rain) and 36 mm·h^{-1} (moderate rain), the SNR decreased sharply. In Fig. 8(b), the SNR of the WindCube V2 DWL in Zhoushan and Taizhou decreased with the increase of *I*. During the study period, the precipitation was mostly in the sunny class, followed by light rain. The above analyses show that the SNR of WindPrint S4000 DWL at high levels is easily affected by *I*, while the SNR of WindCube V2 DWL at all observation heights is greatly affected by *I*.

https://doi.org/10.5194/amt-2021-42
Preprint. Discussion started: 4 March 2021

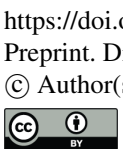

Atmospheric Measurement Techniques Discussions

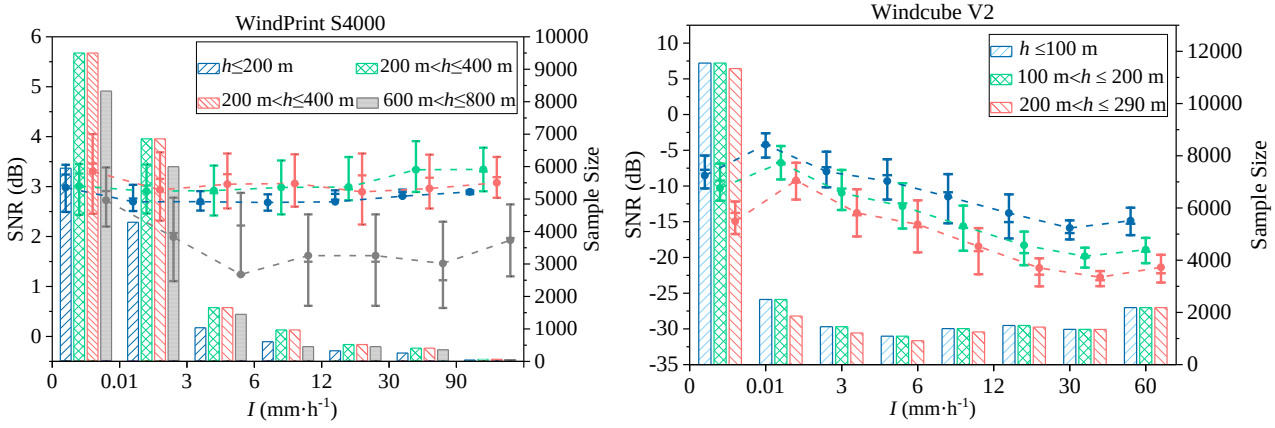

(a) (b)

Figure 8: The box plot of signal-to-noise ratio (SNR) of DWL changes with precipitation intensity (*I*) for (a) WindPrint S4000 DWL at Baoshan and (b) WindCube V2 DWL at Zhoushan and Taizhou observation points. The histogram represents the sample size. The whisker ends represent the 25th and 75th percentile values of the distribution, the horizontal line in the middle denotes the median value and the solid dot represent the mean value. The precipitation intensity ranges are 0–0.01 mm·h^{-1} (sunny), 0.01–3 mm·h^{-1} (light rain), 3–6 mm·h^{-1} (moderate rain), 6–12 mm·h^{-1} (heavy rain), 12–30 mm·h^{-1} (rainstorm), 30–90 mm·h^{-1} (heavy rainstorm) and above 90 mm h^{-1} (severe rainstorm).

Figure 9 shows the variation of the DWL 1-min data missing rate with the SNR at Baoshan, Zhoushan and Taizhou observation points. Except for the Taizhou observation point, the data missing rate decreased with the increase of the SNR, and the higher the ground height was, the greater the data missing rate became. As shown in Fig. 9(a), the data missing rate of the WindPrint S4000 DWL at the Baoshan observation point was less than 40% below 400 m. When the SNR exceeded 1 dB, the data missing rate was less than 20%. However, the data missing rate above 600 m was high—when the SNR was less than 4 dB, the data missing rate was as high as 100%. In Fig. 9(b), the data missing rate of WindCube V2 decreased with the increase of the SNR, and the data missing rate of the lower layer was clearly less than that of the higher layer. When the SNR was greater than −10 dB, the data missing rate at each height remained at less than 5%. When the SNR was lower than −15 dB, the data missing rate of each layer began to increase significantly. Inspection of Fig. 9(c) shows that the data missing rate of WindCube V2 DWL at the Taizhou observation point did not change significantly with the SNR. In general, except for the Taizhou observation point, the data missing rate of DWL showed a decreasing trend with the increase of the SNR.

https://doi.org/10.5194/amt-2021-42
Preprint. Discussion started: 4 March 2021

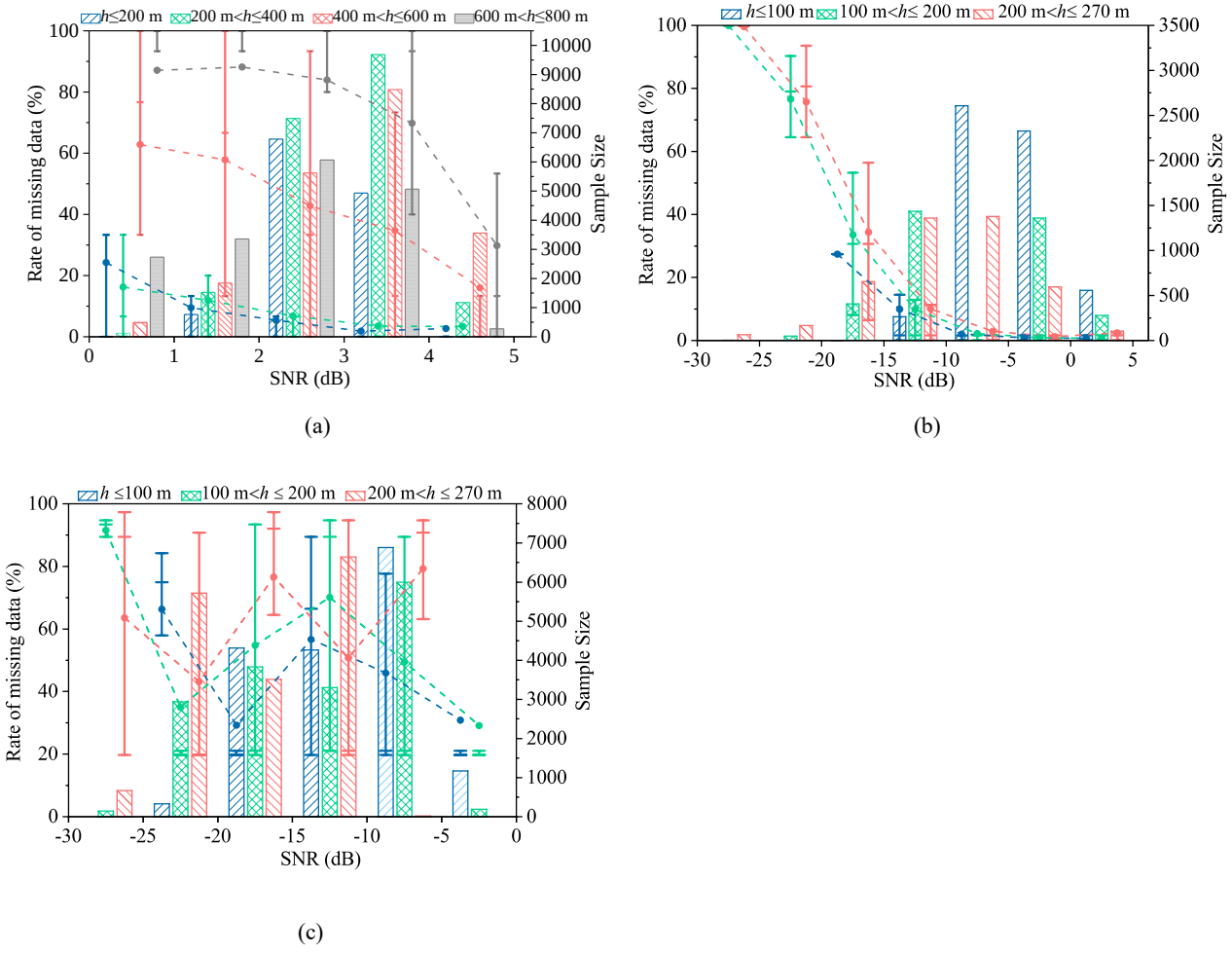

Figure 9: The number of samples and the box plot of rate of missing DWL data changes with the signal-to-noise ratio (SNR) at (a) Baoshan, (b) Zhoushan and (c) Taizhou observation points, respectively. The histogram represents the sample size. The whisker ends represent the 25th and 75th percentile values of the distribution, the horizontal line in the middle denotes the median value and the solid dot represent the mean value.

5.2 Humidity

The water vapor content in the atmosphere has a great influence on the optical properties of aerosols (Beyersdorf et al, 2016; Qiu and Shu, 2017), especially the attenuation of infrared radiation through absorption and scattering in the atmosphere (Eidels-Dubovoi, 2002). Doppler lidar directly measures the Doppler frequency shift generated by the laser beam when atmospheric aerosol particles and atmospheric molecules are scattered, and then inverts the radial wind speed. Therefore, to

https://doi.org/10.5194/amt-2021-42
Preprint. Discussion started: 4 March 2021

Atmospheric Measurement Techniques Discussions

study the influence of the concentration of water vapor molecules in the air, Fig. 10 shows the variation of DWL wind speed and wind direction bias with RH at Baoshan, Zhoushan and Taizhou. Figure 10(a) shows that the influence of humidity on the DWL-measured wind speed was mainly concentrated in RH>85%. When RH>85%, the wind speed bias increased sharply, and the maximum value exceeded 7 $m \cdot s^{-1}$. When RH<85%, the wind speed bias was less than 3 $m \cdot s^{-1}$. As for the wind direction, Fig. 10(b) indicates that starting from RH>85%, the DWL-measured wind direction was gradually affected by humidity. When RH was greater than 90%, the DWL wind direction bias increased sharply, and the maximum value exceeded 60°. When RH was less than 85%, the DWL wind direction bias was relatively small, within 10°. This shows that with an RH>85%, the DWL-measured wind field may have a large deviation, and with an RH<85%, the DWL-measured wind fields are more accurate.

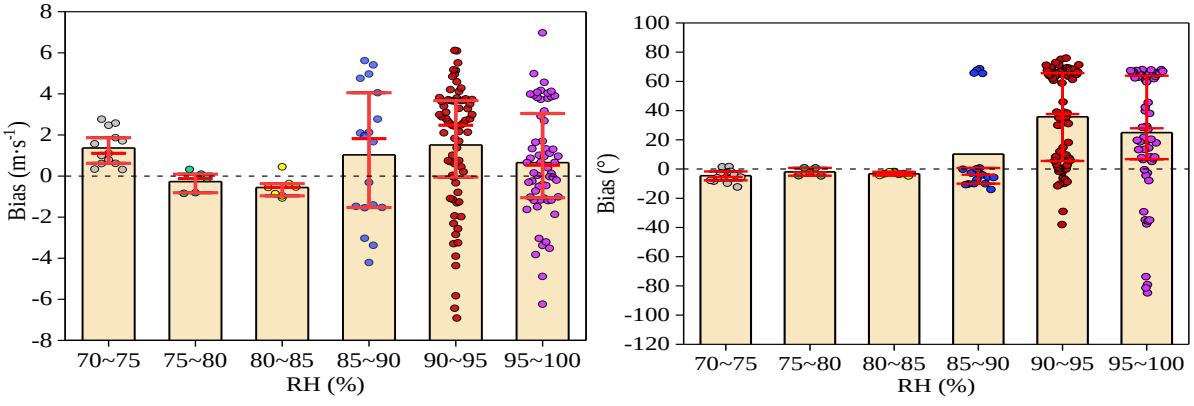

(a) (b)

Figure 10: The sample size and box plot of the DWL-derived (a) wind speed bias and (b) wind direction bias as a function of relative humidity (RH). The histogram represents the average value. The whisker ends represent the 25th and 75th percentile values of the distribution, and the horizontal short line in the middle denotes the median value.

5.3 Drift distance of sounding balloon

As mentioned in Section 4.1, the wind speeds observed by the DWL and the sounding balloons were not strictly in situ observations. The sounding balloons drifted with the wind during the ascent and gradually moved away from the release point. Therefore, there was a deviation between the sounding wind speed observations and the DWL observations. To reveal the relationship between the drift distance of sounding balloon (l_{drift}) and the DWL wind speed and wind direction deviation, Fig. 11 shows the variation of the DWL wind speed and wind direction bias with the sounding balloon drift distance at the Baoshan

https://doi.org/10.5194/amt-2021-42
Preprint. Discussion started: 4 March 2021

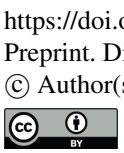

Atmospheric Measurement Techniques Discussions

observation point. It demonstrates that the wind speed bias generally decreased at first and then increased with l_{drift}. Within 1 km, the wind speed bias decreased with the increase of l_{drift}. In the range of 1–1.5 km, the average wind speed bias was approximately equal to zero. When the drift distance exceeded 1.5 km, the wind speed bias increased sharply, and the maximum value of the average wind speed bias exceeded 1.5 $m \cdot s^{-1}$. From Fig. 11(b), the wind direction bias of DWL did not change much with the drift distance of sounding balloon. This shows that the influence of l_{drift} on the DWL wind speed and wind direction deviation differed, and was mainly concentrated in l_{drift}>1.5 km. The wind direction deviation was not affected by l_{drift}.

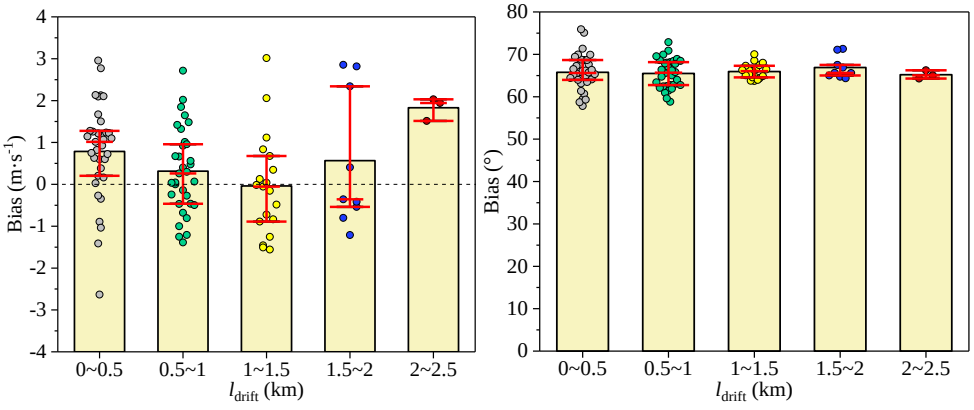

(a) (b)

Figure 11: The sample size and box plot of the DWL-derived (a) wind speed bias and (b) wind direction bias as a function of drift distance of sounding balloon (l_{drift}). The histogram represents the average value. The whisker ends represent the 25th and 75th percentile values of the distribution, and the horizontal short line in the middle denotes the median value.

5.4 Position relative to the typhoon center

To show the influence of the position relative to the typhoon center on the DWL-measured wind speed, the DWL data were divided into two groups according to the observation height, h<200 m and h>200 m. The RMS of each group of data and the measured wind speed of the sounding balloon at the same time and at the same height were calculated. There were five sounding datasets from the Baoshan observation point, nine from Zhoushan, and three from the Taizhou observation point. Fig. 12 depicts the variation in the RMS of wind speed between DWL and radiosonde measurements with the position relative to the typhoon center. The figure indicates that within the range of 0–700 km at both h<200 m and h>200 m, the RMS increased

https://doi.org/10.5194/amt-2021-42
Preprint. Discussion started: 4 March 2021

Atmospheric Measurement Techniques Discussions

as the distance from the typhoon center decreased. The RMS of the Baoshan and Taizhou points was relatively small, and the maximum value did not exceed 2 $m \cdot s^{-1}$. Considering Fig. 4 (a), (b), (e), (f), this may be due to the fact that the Baoshan and Taizhou observation points were far from the typhoon center at the corresponding time, and the wind speed and precipitation intensity were both small. The RMS of the observation point in Zhoushan increased significantly, and the maximum value was 5.89 $m \cdot s^{-1}$ when h<200 m (the corresponding time was 02:22 on August 10, 179 km away from the center of the typhoon, with a corresponding wind speed of 25 $m \cdot s^{-1}$).When h>200 m, the maximum RMS value was 5.78 $m \cdot s^{-1}$ (the corresponding time was 11:50 on August 10, 225 km from the center of the typhoon, and the corresponding wind speed was 16 $m \cdot s^{-1}$). The Zhoushan observation point was relatively closer to the typhoon center (within 250 km). In addition, Fig. 4(c) and (d) demonstrate that at the corresponding time, the wind speed and precipitation intensity of the Zhoushan observation point were much larger than those of the Baoshan and Taizhou observation points. This showed that when the distance from the typhoon center exceeded 250 km, the DWL was less affected, and the RMS was basically less than 2 $m \cdot s^{-1}$. Within a radius of 250 km, the RMS increased significantly as the distance decreased and the RMS reached a maximum of 5.89 $m \cdot s^{-1}$.

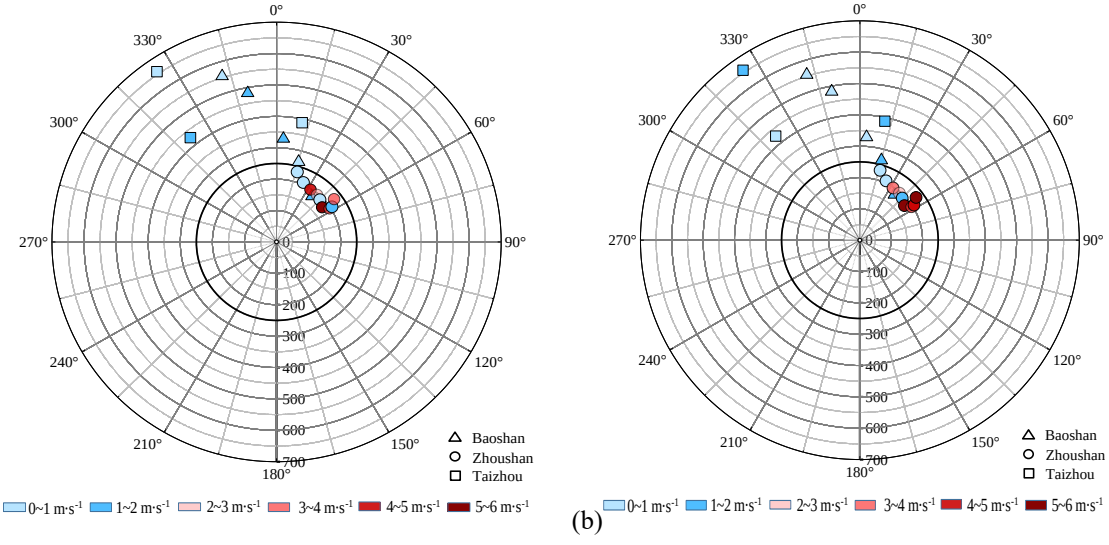

Figure 12: Variation of root mean square (RMS) of wind speed between DWL and radiosonde measurements with the position of the typhoon center. (a) height <200 m and (b) height >200 m The triangle represents the Baoshan observation point, the circle represents the Zhoushan observation point, and the square represents the Taizhou observation point.

https://doi.org/10.5194/amt-2021-42
Preprint. Discussion started: 4 March 2021


Atmospheric Measurement Techniques Discussions

6 Conclusions

This study was based on the joint observations of Super Typhoon Lekima in 2019 by the Shanghai Typhoon Institute of China Meteorological Administration in Baoshan, Zhoushan and Taizhou. The performance of the DWL-measured wind field under typhoon conditions was evaluated, and the impact of precipitation intensity, relative humidity, drift distance of sounding balloons and the position relative to the typhoon center on the DWL wind measurements was studied. In this study, we selected the DWL-measured 30-s, 1-min, and t_{GPS} average wind speeds and directions to evaluate the coincidence degree with the measured instantaneous wind speed of sounding balloons, and we analyzed the impact factors that caused the deviation of the DWL wind field measurement. The research height was 0–600 m.

Through comparing the horizontal wind speed between the DWL and sounding balloon measurements, when the height was below 100 m, the wind speed value observed by the sounding balloon was basically lower than the true wind speed value because of the acceleration when the sounding balloon was released. This resulted in a significant difference of the measured wind speed between the DWL and sounding balloon. Therefore, this paper suggests that the measured wind speed data of sounding balloons below 100 m is not reliable. Comparing the deviation statistics of the average wind speed of the DWL, the 1-min average wind speed of WindPrint S4000 was in the best agreement with the measured instantaneous wind speed of sounding balloons. In the range of 100–600 m, its R was 0.98 and its RMS was 1.29 m s^{-1}. In comparison, the t_{GPS} average wind speed of WindCube V2 was in the best agreement with the instantaneous wind speed of sounding balloons. In the range of 100–290 m, its R was 0.82 and 0.90, and its RMS was 2.19 m s^{-1} and 1.52 m·s^{-1} in Zhoushan and Taizhou, respectively. The DWL-measured horizontal wind direction was in good agreement with the sounding balloon measurement—R exceeded 0.7, and the RMS was less than 15°.

By analyzing the influence of precipitation intensity on the DWL-derived SNR, data missing rate and wind speed deviation, it was seen that the SNR decreased with the increase of *I*. Generally, DWL had poor applicability when I>50 mm·h^{-1}. The precipitation intensity had a large impact on the SNR of WindPrint S4000 above 600 m and at all observation heights of WindCube V2. The rate of missing DWL data increased with an increase of *I*. Moreover, the data missing rate of the lower layer, which was not affected much by *I* and remained within 20%, was significantly smaller than that of the higher layer.

There was an obvious correlation between the DWL wind speed bias and the RH. When the RH was less than 85%, the

https://doi.org/10.5194/amt-2021-42
Preprint. Discussion started: 4 March 2021


Atmospheric Measurement Techniques Discussions

DWL wind speed bias was small (less than 3 $m \cdot s^{-1}$). When the RH exceeded 85%, the DWL wind speed bias increased sharply, and the maximum value exceeded 7 $m \cdot s^{-1}$. The influence of RH on DWL-measured wind direction was mainly concentrated around RH>90%, and the maximum wind direction bias exceeded 60°. In addition, the DWL wind speed bias generally decreased with the increase of l_{drift} within 1 km. When it exceeded 1.5 km, the wind speed bias increased sharply with the average value exceeded 1.5 $m \cdot s^{-1}$. In comparison, the DWL wind direction observation was not strongly affected by l_{drift}.

Within a radius of 700 km, the RMS of wind speeds between DWL and sounding balloon measurements showed a trend of increasing as the distance from the typhoon center decreased. Beyond 250 km from the typhoon center, the RMS was less than 2 $m \cdot s^{-1}$. Within a radius of 250 km, the RMS increased significantly with the decrease of distance, and the maximum RMS reached 5.89 $m \cdot s^{-1}$.

Acknowledgments

This work was supported by the National Key R&D Program of China (No. 2018YFB1501104), the National Natural Science Foundation of China (No. 41805088), Natural Science Foundation of Shanghai (No. 18ZR1449100). We thank Leonie Seabrook, PhD, from Liwen Bianji, Edanz Editing China, for editing the English text of a draft of this manuscript.

References

[1] Barat, J., and Cot, C.: Accuracy analysis of Rubsonde-GPS wind sounding system, J. Appl. Meteorol., 34, 1123-1132, doi:10.1175/1520-0450(1995)034<1123:AAORGW>2.0.CO;2, 1995.

[2] Beyersdorf, A. J., Ziemba, L. D., Chen, G., Corr, C. A., Crawford, J. H., Diskin, G. S., Moore, R. H., Thornhill, K. L., Winstead, E. L., and Anderson, B. E.: The impacts of aerosol loading, composition, and water uptake on aerosol extinction variability in the Baltimore-Washington, DC region, Atmos. Chem. Phys., 16, 1003-1015, doi:10.5194/acp-16-1003-2016, 2016.

[3] Bucci, L. R., O'Handley, C., Emmitt, G. D., Zhang, J. A., Ryan, K., and Atlas, R.: Validation of an airborne doppler wind lidar in tropical cyclones, Sensors-Basel, 18, ARTN4288, doi:10.3390/s18124288, 2018.

[4] Courtney, M., Wagner, R., and Lindelow, P.: Testing and comparison of lidars for profile and turbulence measurements in wind energy, Iop C. Ser. Earth Env. Sci., 1, U172-U185, doi:10.1088/1755-1315/1/1/012021, 2008.

[5] Davis, J., Collier, C., Davies, F., Burton, R., Pearson, G., and Di Girolamo, P.: Vertical velocity observed by Doppler lidar during cops - A case study with a convective rain event, Meteorol. Z., 22, 463-470, doi:10.1127/0941-2948/2013/0411, 2013.

[6] Drew, D. R., Barlow, J. F., and Lane, S. E.: Observations of wind speed profiles over Greater London, UK, usinga Doppler lidar, J. Wind Eng. Ind. Aerod., 121, 98-105, doi:10.1016/j.jweia.2013.07.019, 2013.

[7] Eidels-Dubovoi, S.: Aerosol impacts on visible light extinction in the atmosphere of Mexico City, Sci. Total Environ., 287, 213-220, Pii S0048-9697(01)00983-4, doi:10.1016/S0048-9697(01)00983-4, 2002.

[8] Gasch, P., Wieser, A., Lundquist, J. K., and Kalthoff, N.: An LES-based airborne Doppler lidar simulator and its application to wind profiling in inhomogeneous flow conditions, Atmos. Meas. Tech., 13, 1609-1631, doi:10.5194/amt-13-1609-2020, 2020.

[9] Holleman, I.: Quality control and verification of weather radar wind profiles, J. Atmos. Ocean Tech., 22, 1541-1550, doi:10.1175/Jtech1781.1, 2005.

[10] Hughes, A. J., O'Shaughnessy, J., Pike, E. R., McPherson, A., Spavins, C., and Clifton, T.H.: Long range anemometry using a CO_2 laser, Opto-electronics, 4, 379-384, doi:10.1007/BF01414142, 1972.

[11] Köpp, F., Schwiesow, R., and Werner, C.: Remote measurements of boundary-layer wind profiles using a CW Doppler lidar, J. APPL. METEOROL., 23, 148-154, doi:10.1175/1520-0450(1984)023<0148:RMOBLW>2.0.CO;2, 1984.

[12] Laurence Korb, C., Gentry, B. M., and Weng, C. Y.: Edge technique: Theory and application to the lidar measurement of atmospheric wind, Appl. Optics, 31, 4202-4213, doi:10.1364/AO.31.004202, 1992.

[13] Kumer, V. M., Reuder, J., and Furevik, B. R.: A comparison of LiDAR and radiosonde wind measurements, Enrgy. Proced., 53, 214-220, doi:10.1016/j.egypro.2014.07.230, 2014.

[14] Laurence Korb, C., Gentry, B. M., and Weng, C. Y.: Edge technique: Theory and application to the lidar measurement of atmospheric wind, Appl. Optics, 31, 4202-4213, doi:10.1364/AO.31.004202, 1992.

[15] Lambert, W., and Taylor, G.: Data Quality Assessment Methods for the Eastern Range 915 MHz Wind Profiler Network,

https://doi.org/10.5194/amt-2021-42
Preprint. Discussion started: 4 March 2021


Atmospheric Measurement Techniques Discussions

Kennedy Space Center, Florida, NASA Contractor Report CR-1998-207906, 49, vailable from [NSCO, Inc., 1980 N. Atlantic Ave., Suite 230, Cocoa Beach, FL 32931], 1998.

[16] Li, J. L., and Yu, X.: LiDAR technology for wind energy potential assessment: Demonstration and validation at a site around Lake Erie, Energ. Convers. Manage., 144, 252-261, doi:10.1016/j.enconman.2017.04.061, 2017.

[17] Li, J. L., Wang, X. F., and Yu, X.: Use of spatio-temporal calibrated wind shear model to improve accuracy of wind resource assessment, Appl. Energ., 213, 469-485, doi:10.1016/j.apenergy.2018.01.063, 2018.

[18] Li, J. L., and Yu, X.: Onshore and offshore wind energy potential assessment near Lake Erie shoreline: A spatial and temporal analysis, Energy, 147, 1092-1107, doi:10.1016/j.energy.2018.01.118, 2018.

[19] Li, S. H., Sun, X. J., Zhang, R. W., and Zhang, C. L.: Simulation of Frequency Discrimination and Retrieval of Wind Speed for the Bistatic Doppler Wind Lidar, Optik, 179, 796-803, doi:10.1016/j.ijleo.2018.10.122, 2019.

[20] Li, Y., Wang, B. M., Lee, S. Y., Zhang, Z. J., Wang, Y., and Dong, W. J.: Micro-Pulse Lidar Cruising Measurements in Northern South China Sea, Remote Sens., 12, ARTN 1695, doi:10.3390/rs12101695, 2020.

[21] Powell, M. D., Vickery, P. J., and Reinhold, T. A.: Reduced drag coefficient for high wind speeds in tropical cyclones, Nature, 422, 279-283, doi:10.1038/nature01481, 2003.

[22] Pu, Z. X., Zhang, L., and Emmitt, G. D.: Impact of airborne Doppler wind lidar profiles on numerical simulations of a tropical cyclone, Geophys. Res. Lett., 37, Artn L05801, doi:10.1029/2009gl041765, 2010.

[23] Qiu, Y. J., and Shu, Z. Z.: The effect of relative humidity on the tropospheric aerosol extinction coefficient with typical underlying surfaces based on CALIPSO data, Int. J. Remote Sens., 39, 276-288, doi:10.1080/01431161.2017.1371860, 2018.

[24] Ralph, F. M., Neiman, P. J., Van De Kamp, D. W., and Law, D. C.: Using spectral moment data from NOAA's 404–MHz radar wind profilers to observe precipitation, Bull. Am. Meteorol. Soc., 76, 1717-1739, doi:10.1175/1520-0477(1995)076<1717: USMDFN>2.0.CO;2, 1995.

[25] Roadcap, J. R., McNicholl, P. J., Teets, E. H., and Laird, M. H.: Comparison of CO_2 Doppler lidar and GPS rawinsonde wind velocity measurements, P. Soc. Photo-Opt. Ins., 4376, 141-152, doi:10.1117/12.438174, 2001.

[26] Smith, R. K., and Montgomery, M. T.: Hurricane boundary-layer theory, Q. J. Roy. MeteorSoc., 136, 1665-1670,

doi:10.1002/qj.679, 2010.

[27] T/CMSA0013-2019.: The grade of rainfall in short time weather service (in Chinese), China Meteorological Service Association, Beijing, available at: http://www.chinamsa.org/uploads/file/20191106142922_61962.pdf, 2019.

[28] Tang, S. M., Guo, Y., Wang, X., Tang, J., Li, T. T., Zhao, B. K., Zhang, S., and Li, Y. P.: Validation of Doppler Wind Lidar during Super Typhoon Lekima (2019), Front. Earth Sci., doi:10.1007/s11707-020-0838-9, 2020.

[29] Träumner, K., Wieser, A., Grenzhäuser, J., and Kottmeierr, C.: Advantages of a coordinated scanning Doppler lidar and cloud radar system for wind measurements, Fourth symposium on lidar atmospheric applications, Arizona, available at: http://ams.confex.com/ams/89annual/techprogram/paper_146092.htm, 2009.

[30] Wolfe, D., Fairall, C., Intrieri, J., Ratterree, M., and Tucker, S.: Shipboard multisensor wind profiles from NEAQS 2004: radar wind profiler, high resolution Doppler lidar, GPS rawinsonde, 13th Symposium on Meteorological Observations and Instrumentation, Joint Poster Session JP2, available at: https://ams.confex.com/ams/pdfpapers/92496.pdf, 2005.

[31] Ying, M., Zhang, W., Yu, H., Lu, X. Q., Feng, J. X., Fan, Y. X., Zhu, Y. T., and Chen, D. Q.: An Overview of the China Meteorological Administration Tropical Cyclone Database, J. Atmos. Ocean Tech., 31, 287-301, doi:10.1175/Jtech-D-12-00119.1, 2014.

[32] Zhang, J. A., Atlas, R., Emmitt, G. D., Bucci, L., and Ryan, K.: Airborne Doppler Wind Lidar Observations of the Tropical Cyclone Boundary Layer, Remote Sens., 10, ARTN 825, doi:10.3390/rs10060825, 2018.

[33] Zheng, C., Gao, Z., Rui, Z., and Chen, X.: Application of T639 forecasting wind field around Taiwan island, Journal of PLA University of Science and Technology (Natural Science Edition), 16, 80-88, doi:10.7666/j.issn.1009-3443.201408010, 2015.